

RESEARCH LETTER

10.1002/2016GL070003

Special Section:

First results from NASA's Magnetospheric Multiscale (MMS) Mission

Key Points:

- The MMS spacecraft configuration, orbits, and data resolution enable us to ascertain magnetopause (wave) inclinations with high accuracy
- Inverse wave steepening (steeper trailing edges) occurs also when the IMF is in the GSM x-y plane, not only during mainly northward IMF
- Inverse steepening may be associated to the absence of KHI or to instabilities from the alignment of flow and magnetic fields in the sheath

Supporting Information:

- Supporting Information S1
- Data Set S1

Correspondence to:

F. Plaschke,
Ferdinand.Plaschke@oeaw.ac.at

Citation:

Plaschke, F., et al. (2016), Steepening of waves at the duskside magnetopause, *Geophys. Res. Lett.*, 43, 7373–7380, doi:10.1002/2016GL070003.

Received 20 JUN 2016

Accepted 8 JUL 2016

Accepted article online 13 JUL 2016

Published online 25 JUL 2016

Steepening of waves at the duskside magnetopause

F. Plaschke¹, N. Kahr¹, D. Fischer¹, R. Nakamura¹, W. Baumjohann¹, W. Magnes¹, J. L. Burch², R. B. Torbert^{2,3}, C. T. Russell⁴, B. L. Giles⁵, R. J. Strangeway⁴, H. K. Leinweber⁴, K. R. Bromund⁵, B. J. Anderson⁶, G. Le⁵, M. Chutter³, J. A. Slavin⁷, and E. L. Kepko⁵

¹Space Research Institute, Austrian Academy of Sciences, Graz, Austria, ²Southwest Research Institute, San Antonio, Texas, USA, ³Institute for the Study of Earth, Oceans, and Space, University of New Hampshire, Durham, New Hampshire, USA, ⁴Department of Earth, Planetary, and Space Sciences, University of California, Los Angeles, California, USA, ⁵NASA Goddard Space Flight Center, Greenbelt, Maryland, USA, ⁶The Johns Hopkins University Applied Physics Laboratory, Laurel, Maryland, USA, ⁷Department of Climate and Space Sciences and Engineering, University of Michigan, Ann Arbor, Michigan, USA

Abstract Surface waves at the magnetopause flanks typically feature steeper, i.e., more inclined leading (antisunward facing) than trailing (sunward facing) edges. This is expected for Kelvin-Helmholtz instability (KHI) amplified waves. Very rarely, during northward interplanetary magnetic field (IMF) conditions, anomalous/inverse steepening has been observed. The small-scale tetrahedral configuration of the Magnetospheric Multiscale spacecraft and their high time resolution measurements enable us to routinely ascertain magnetopause boundary inclinations during surface wave passage with high accuracy by four-spacecraft timing analysis. At the dusk flank magnetopause, 77%/23% of the analyzed wave intervals exhibit regular/inverse steepening. Inverse steepening happens during northward IMF conditions, as previously reported and, in addition, during intervals of dominant equatorial IMF. Inverse steepening observed under the latter conditions may be due to the absence of KHI or due to instabilities arising from the alignment of flow and magnetic fields in the magnetosheath.

1. Introduction

The geomagnetic field is enclosed by the magnetopause (MP) boundary that separates the inner magnetosphere from the magnetosheath region [e.g., Cahill and Amazeen, 1963]. Within that region, the decelerated and thermalized solar wind plasma flows around the obstacle that the geomagnetic field constitutes [e.g., Spreiter et al., 1966]. The magnetic field in the magnetosheath is given by the draped interplanetary magnetic field (IMF). Changes in magnetic field across the dayside MP are accounted for by the so-called Chapman-Ferraro current [Chapman and Ferraro, 1930].

The average location of the MP is determined by pressure balance [e.g., Sibeck et al., 1991], but around that location, the MP is always in motion. It is a highly dynamic boundary even under steady upstream conditions. Consequently, surface waves are frequently observed to propagate along the MP [e.g., Song et al., 1988]. On the flanks, these surface waves typically move tailward, due to the antisunward plasma motion in the magnetosheath. The shear flow across the MP may cause the waves to grow in amplitude, due to the Kelvin-Helmholtz instability (KHI). While growing nonlinearly in amplitude, the leading edges of the waves are steepened until the waves break and evolve into vortices [see Li et al., 2012]. Throughout this paper, the term “steepening” refers to the shape of the MP boundary and not to the gradients in magnetic field and particle moments, which are larger at the trailing (sunward) edges of KHI amplified waves [e.g., Hasegawa et al., 2004; Nakamura et al., 2004]. Observations of Kelvin-Helmholtz waves (KH waves) at the MP and simulations showing steeper leading edges of those waves are abundant [e.g., Fairfield et al., 2000; Foullon et al., 2008; Li et al., 2013]; a recent review about waves on the MP can be found in Plaschke [2016].

By contrast, MP surface waves featuring anomalous inverse steepening, i.e., steeper trailing edges, have only been observed in very rare occasions. Hence, little is known about waves of this type, e.g., how they develop. Chen et al. [1993] and Chen and Kivelson [1993] report observations of such surface waves at the dawn flank MP by the ISEE 1 and 2 spacecraft that took place during two intervals of persistently northward IMF conditions. Under these conditions, a plasma depletion layer of decreased plasma density and enhanced magnetic field may form at the subsolar MP, as reconnection is suppressed [Sibeck et al., 1990]. Flux tubes and plasma

within this layer can strongly accelerate along the equatorial flanks of the MP toward the tail due to magnetic pressure gradient and tension forces [Lavraud *et al.*, 2007]. Chen *et al.* [1993] and Chen and Kivelson [1993] hypothesize that it is this accelerating motion of plasma and magnetic field that caused the inverse steepening of the waves by dragging the trailing edges in tailward direction. In this picture, the magnetic field in the magnetosheath shapes the waves.

Plaschke *et al.* [2013] discuss another case of inversely steepened MP surface waves, observed by the inner Time History of Events and Macroscale Interactions during Substorms (THEMIS) spacecraft [Angelopoulos, 2008] at the dayside dusk flank, also under strongly northward IMF conditions. However, the magnetic field in the magnetosheath was not aligned with the phase fronts of the surface waves. Furthermore, magnetosheath plasma was also moving slower than the wave within inward MP indentations. Both observations contrast with the suggested generation mechanism of inverse MP wave steepening.

The importance of the inversely steepened MP surface waves stems from the resulting enhanced transfer of momentum to the plasma inside the MP and the inner magnetospheric consequences of that viscous interaction [e.g., Farrugia *et al.*, 2001]. It is, hence, desirable to understand under which upstream conditions inverse steepening takes place and, ultimately, how it is caused. A prerequisite for the identification of inversely steepened MP surface waves is the ability to determine local boundary normal directions by spacecraft accurately, to within a few degrees, on passage of a surface wave, in a routine manner. This can be achieved by the four-spacecraft timing method [e.g., Harvey, 1998] if the MP can be assumed to be planar on the scales of the (ideally tetrahedral) spacecraft configuration. As MP surface wave amplitudes may be low, on the order of 1000 km [see, Chen and Kivelson, 1993; Plaschke *et al.*, 2013], spacecraft distances need to be lower than that at least by an order of magnitude.

The Magnetospheric Multiscale (MMS) spacecraft routinely achieve the required configuration, for the first time [Burch *et al.*, 2016]. The four MMS spacecraft were launched in March 2015 into a common, highly elliptical, equatorial orbit around Earth. The first science phase started on 1 September 2015. Within this phase, the spacecraft are flying in tetrahedral configuration around apogee (at $12 R_E$ from Earth), featuring interspacecraft distances on the order of 10 to 100 km. Between September and November 2015, the spacecraft traversed the equatorial, dayside dusk flank MP almost on each orbit. This MMS data set gives us the unique opportunity to routinely characterize MP surface waves with respect to their shape and, thereby, to make a step forward in understanding the phenomenon of inverse MP surface wave steepening.

2. Data Analysis

The main data source for this study is a set of “merged” magnetic field measurements, composed by combination of burst mode FluxGate Magnetometer (FGM) [Russell *et al.*, 2016] and Search Coil Magnetometer (SCM) data [Le Contel *et al.*, 2016]. The MMS magnetometers are part of the FIELDS instrument suite [Torbert *et al.*, 2016]. The resolution of the FGM and SCM data is 128 Hz and 8192 Hz, respectively. By nature of the instruments, the FGM measurements are particularly accurate in the low-frequency range, while the SCM signal-to-noise ratio is very low under ~ 0.1 Hz. We need magnetic field data with high time resolution that include the lowest-frequency part of the spectrum. The merged magnetic field data product fulfills these requirements. It features a resolution of 1024 Hz which is an order of magnitude higher than the FGM resolution. The exact details of the merging process are explained in Fischer *et al.* [2016].

High time resolution data are necessary to achieve the desired accuracy on using the timing method for boundary normal determination [Harvey, 1998]. The angular error Δn in the normal vector may be estimated by

$$\Delta n = \arcsin\left(\frac{v \Delta t}{S}\right) \quad (1)$$

where v is the boundary velocity, Δt is timing uncertainty, and S is the scale size of the spacecraft configuration. From October to December 2015, the MMS tetrahedral spacecraft configuration size was on the order of $S = 10$ km. Furthermore, MP boundary velocities can easily reach and exceed $v = 300$ km/s. With these values, we obtain $\Delta n = 13.6^\circ$ and 1.7° for $\Delta t = (1/128)$ s and $(1/1024)$ s, the sampling periods of burst FGM and merged magnetic field measurements, respectively. Clearly, high accuracies in normal vector direction can only be achieved by using the merged magnetic field measurements; the FGM burst measurements alone are insufficient. Merged data are available for burst intervals in September, October, and November 2015.

We are interested in MP crossings by the four MMS spacecraft during these months. Intervals encompassing (partial) MP crossings are selected by visual inspection of magnetic field and omnidirectional ion spectral energy density measurements by the Fast Plasma Investigation (FPI) instruments [Pollock *et al.*, 2016]. In the latter measurements, MP crossings are visible in a change between magnetospheric and magnetosheath populations, at energies of ~ 10 keV and ~ 1 keV, respectively. This can be seen in Figure S1 (top) in the supporting information. The figure shows an example interval of MMS 1 observations encompassing several MP crossings. We manually selected ~ 1000 intervals around such MP crossings, for which merged magnetic field measurements are available for all four spacecraft. A list of times and other quantities pertaining to these crossings can be found in the supporting information as well.

The time lags of the magnetic field signatures between spacecraft pairs (MMS 1 and 2, 1 and 3, and 1 and 4) are obtained by a cross-correlation method that involves all three magnetic field components (in geocentric solar ecliptic coordinates, GSE). Let $\bar{B}_2(t)$ be the magnetic field time series measured by MMS 2 within a selected interval and $\bar{B}_1(t + \tau)$ a time series from MMS 1 pertaining to an interval of equal length but time shifted by τ . We subtract component wise the mean, e.g., $\tilde{B}_{1x}(t + \tau) = B_{1x}(t + \tau) - \bar{B}_{1x}(\tau)$, where $\bar{B}_{1x}(\tau)$ is the mean over the entire interval. Subsequently, we compute the cross-correlation coefficient as follows:

$$P_{12}(\tau) = \frac{\sum_t (\tilde{B}_1(t + \tau) \cdot \tilde{B}_2(t))}{\sqrt{(\sum_t \tilde{B}_1^2(t + \tau)) (\sum_t \tilde{B}_2^2(t))}}. \quad (2)$$

The time lag τ_{12} between MMS 1 and MMS 2 signatures is then given by τ for which P_{12} maximizes. From the lag times τ_{12} , τ_{13} , and τ_{14} we obtain a local boundary normal vector \vec{n} and the boundary velocity v along that vector by four-spacecraft timing analysis, as detailed in section 12.1.2 of Harvey [1998]. It should be noted that the normal vectors \vec{n} point in the direction of local MP motion, i.e., toward the magnetosheath for inbound crossings of the MP by the spacecraft (magnetosheath to magnetosphere) and toward the magnetosphere for outbound crossings (magnetosphere to magnetosheath).

The vectors \vec{n} need to be compared to reference normals, i.e., transformed into reference boundary normal coordinates (LMN). Therefore, solar wind conditions are required. These are obtained from the NASA OMNI data set [King and Papitashvili, 2005], averaged over 5 min preceding the respective times of interest. The OMNI solar wind data are already propagated to the bow shock nose; the additional 5 min account for the propagation through the dayside magnetosheath. We convert the MMS positions into aberrated GSE (AGSE) coordinates, whose x axis is rotated toward $-y$ by $\arctan(v_E/v_{sw})$ with respect to standard GSE. Here v_E denotes the orbital velocity of Earth around the Sun and v_{sw} denotes the solar wind velocity. In this AGSE system, the Shue *et al.* [1998] MP model

$$r = r_0 \left(\frac{2}{1 + \cos \theta} \right)^\alpha \quad (3)$$

yields reference normal directions N at the positions of MMS 1, given by the radial distances to Earth r and the angles θ to AGSE x , at the respective center times of the crossing intervals. The parameter α is a function of the z component of the IMF (B_z) and of the solar wind dynamic pressure (D_p); it is given by equation (11) in Shue *et al.* [1998]. L points northward, perpendicular to the planes given by the respective MMS 1 position vectors and AGSE x . M is directed westward, perpendicular to L and N . We compute angles $\phi = \arctan(-n_M/n_N)$ of \vec{n} with respect to N in the N - M plane, counted positive toward $-M$ (see Figure 1a). As illustrated in Figure 1b that shows expected values of ϕ for waves of different steepening, at the dusk flank MP, inbound crossings of the MP by the spacecraft should generally (but not necessarily always) correspond with angles ϕ between 0° and 90° , whereas outbound crossings should yield ϕ between 90° and 180° . This is, indeed, the case (see also Figure S1 (bottom) in the supporting information).

We further select crossings for which P_{12} , P_{13} , and P_{14} are larger than 0.9; for which the geometry factor $Q_{GM} > 2.7$ [Robert *et al.*, 1998] to ensure a tetrahedral spacecraft configuration; that were seen at the dusk MP, i.e., at positive AGSE y ; and for which we obtained angles ϕ between 0° and 180° corresponding with tailward moving MP surface waves or undulations. In total, 808 crossings fulfill these criteria. We only consider these crossings hereafter.

We group subsequent crossings that happened within 10 min long intervals. Groups should include at least three inbound and three outbound crossings. Different groups should be composed of different sets of

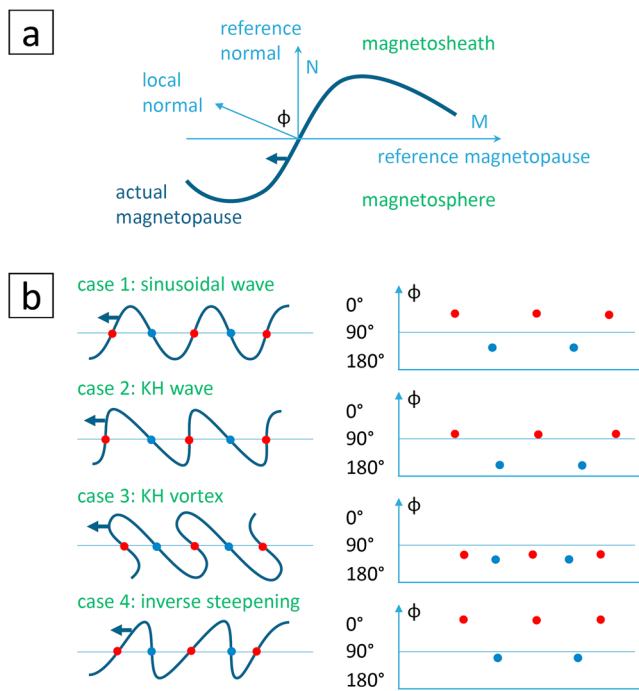


Figure 1. (a) Sketch of the reference N direction and local normal \bar{n} of the MP; \bar{n} always points in the direction of local MP motion. The angle between them in the N - M plane is denoted by ϕ . (b) Different cases of MP wave steepening are illustrated (left column) and the corresponding expected time series of ϕ are shown (right column).

crossings, though we allow partial overlap. Thereby, we obtain 111 groups that contain between 6 (minimum) and 13 crossings. The MP crossings marked in Figure S1 (bottom) (supporting information) belong to one group. We compute average angles $\langle\phi\rangle$ (and standard deviations $\Delta\phi$) pertaining to the inbound and outbound crossings of each group and denote them with $\langle\phi_i\rangle$ and $\langle\phi_o\rangle$. Furthermore, we compute the average angle of $\langle\phi_i\rangle$ and $\langle\phi_o\rangle$ for each group and denote it with $\langle\phi_m\rangle = (\langle\phi_i\rangle + \langle\phi_o\rangle)/2$. That angle should be $>90^\circ$ for regular, KH wave steepening and $<90^\circ$ for inverse steepening. For the example interval of Figure S1, we obtain $\langle\phi_i\rangle = 59.7^\circ$, $\langle\phi_o\rangle = 111.8^\circ$, and $\langle\phi_m\rangle = 85.7^\circ$ (inverse steepening). Finally, average solar wind conditions (IMF, velocity, and density) over all crossings within a group are assigned to that group.

3. Results and Discussion

Based on the 808 selected crossings, the average ϕ over all inbound crossings is 57.6° , and 134.3° for all outbound crossings. The average of these two numbers is 96.0° , which is larger than 90° indicating a tendency toward regular, KH wave steepening (see Figure 1, case 2). The spread in ϕ is very significant, though. The corresponding standard deviations are 31.3° and 23.1° for inbound and outbound crossings, respectively.

Average angles $\langle\phi_i\rangle$, $\langle\phi_o\rangle$, and $\langle\phi_m\rangle$ as defined above for groups of crossings are shown in Figure 2a in red, blue, and black, respectively. Apparently, the ranges of values that $\langle\phi_i\rangle$ and $\langle\phi_o\rangle$ can hold are rather large. We find $\langle\phi_i\rangle$ to be within 31° and 99° and $\langle\phi_o\rangle$ between 109° and 153° . As expected, $\langle\phi_i\rangle$ can also exhibit values above 90° when KH waves break and form vortices, as shown in Figure 1b case 3. That also explains the larger range of values of $\langle\phi_i\rangle$ with respect to $\langle\phi_o\rangle$, which does not come from a higher variability of ϕ_i within groups, as evidenced in Figure 2b: $\Delta\phi$ averages over all groups are very similar for inbound (22.0°) and outbound (21.3°) crossings.

Furthermore, variability in $\langle\phi_i\rangle$ and $\langle\phi_o\rangle$ is also expected (1) from the range of aspect ratios (amplitude versus wave length) that MP surface waves may feature and (2) from the location (along N) at which the spacecraft sense the waves: (1) Smaller/larger $\langle\phi_i\rangle$ and larger/smaller $\langle\phi_o\rangle$ should result from waves of smaller/larger amplitude versus wavelength. This variability should, in principle, not affect $\langle\phi_m\rangle$. (2) Deviations in observation location from the center of the wave along N might affect $\langle\phi_m\rangle$, in particular, if KH waves of case 3 (Figure 1b) are being observed, i.e., KH vortices that are just being formed. Spacecraft observations of the center part of these vortices should lead to $\langle\phi_i\rangle > 90^\circ$. Observations of the outermost or innermost parts,

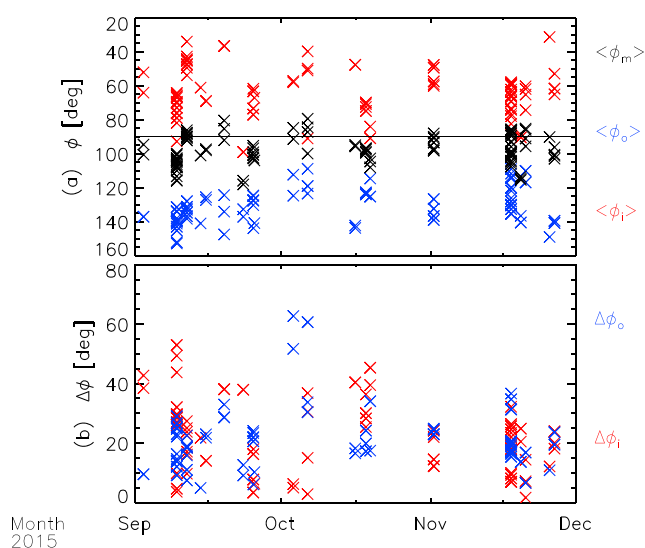


Figure 2. (a) $\langle \phi_i \rangle$ (red), $\langle \phi_o \rangle$ (blue), and $\langle \phi_m \rangle$ (black), pertaining to each of the 111 groups. The times are average times of the crossings in each group. The horizontal line depicts the 90° level. (b) Standard deviations $\Delta \phi$ of the inbound (red) and outbound (blue) ϕ of each group.

however, should result in $\langle \phi_i \rangle < 90^\circ$, and the patterns of observed angles ϕ should be more similar to the patterns expected for cases 2 or even 1 (see Figure 1b, right column). Hence, in general, off-center observations of MP waves should yield $\langle \phi_m \rangle$ closer to 90° .

Indeed, $\langle \phi_m \rangle$ features a lower variability (values between 79° and 118°), as shown by the black crosses in Figure 2a. Most noticeably, values (slightly) larger than 90° (average 98°) are predominant, i.e., they are obtained for 86 out of the 111 groups (77%). Hence, more than three quarters of the MP surface waves dealt with in this study exhibit KH wave type steepening (cases 2 and, much more rarely, 3 in Figure 1b).

We are interested in the other cases, for which $\langle \phi_m \rangle < 90^\circ$, indicating a tendency toward inverse steepening (case 4 in Figure 1b). To identify solar wind conditions that are favorable for inverse MP wave steepening, we plot $\langle \phi_m \rangle$ over the respective solar wind conditions associated to the crossing groups (see Figure S2 in the supporting information). However, there is no one clearly favorable set of solar wind conditions apparent. For instance, $\langle \phi_m \rangle < 90^\circ$ occur for relatively low solar wind velocities below 400 km/s and for high velocities beyond 600 km/s . The most pronounced trends pertain to the IMF components in geocentric solar magnetospheric (GSM) coordinates, and we might get the impression that strongly negative IMF B_x and B_y and strongly positive B_z are favorable for inverse steepening. However, that judgment neglects that some $\langle \phi_m \rangle < 90^\circ$ cases are found for positive B_x , about half of the cases pertain to positive B_y , and a clear majority of $\langle \phi_m \rangle < 90^\circ$ cases was found during negative B_z conditions. IMF clock and cone angles, defined as $\arccos(B_z / \sqrt{B_y^2 + B_z^2})$ and $\arccos(|B_x| / B)$, respectively, do not control $\langle \phi_m \rangle$ either. Also, the observation position along the dusk flank MP given by the angle θ as used in equation (3) is not a good proxy for $\langle \phi_m \rangle$. This latter result is rather unexpected, as KHI-caused steepening should increase toward the tail. Thus, higher θ should correlate with higher $\langle \phi_m \rangle$. We see such a trend, but it is very weak.

Angles $\langle \phi_m \rangle$ seem to be more ordered if plotted against IMF B_z relative to the magnetic field in the x - y plane, i.e., $B_z / \sqrt{B_x^2 + B_y^2}$, as shown in Figure 3.

First, we see in that figure that most groups are associated with negative B_z . The reason is probably a bias on selecting burst intervals for download from the MMS spacecraft. As MMS is a reconnection-focused mission [Burch et al., 2016], MP intervals with reconnection signatures are preferably chosen for the download of high-resolution data. The occurrence of these signatures should correlate with negative IMF B_z . Since we rely on burst magnetic field FGM and SCM data, the IMF conditions of the selected MP crossing intervals are also biased toward negative IMF B_z .

Second, there are a few groups of crossings associated with positive B_z . Most remarkably, two of those groups, for which we obtain $\langle \phi_m \rangle < 90^\circ$ (wave with inverse steepening), pertain to $B_z / \sqrt{B_x^2 + B_y^2} > 2$, i.e., mainly

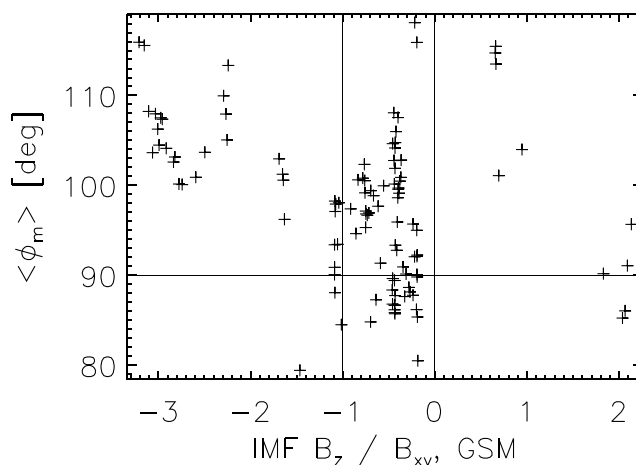


Figure 3. Angles $\langle \phi_m \rangle$ plotted against IMF $B_z / \sqrt{B_x^2 + B_y^2}$ in GSM.

northward IMF. This condition coincides with what was reported by *Chen et al.* [1993], *Chen and Kivelson* [1993], and also *Plaschke et al.* [2013]. Consequently, the driving mechanism suggested by *Chen et al.* [1993] and *Chen and Kivelson* [1993] may be applicable.

Third, the vast majority of inversely steepened waves were observed by MMS during $B_z < 0$ conditions, due to the selection bias detailed above, but $B_z / \sqrt{B_x^2 + B_y^2} > -1$ holds for almost all corresponding groups (between the vertical lines in Figure 3). Also, the group of crossings shown in Figure S1 (supporting information) falls into this category. That is remarkable as quite a number of (regularly steepened) waves were observed under IMF $B_z / \sqrt{B_x^2 + B_y^2} < -1$ conditions. Hence, inversely steepened waves can occur while $B_z < 0$, in particular, if B_z is not the dominant IMF component. The IMF will then predominantly lie in the x-y plane. Within the equatorial magnetosheath, the draped IMF will be mainly perpendicular to the magnetospheric magnetic field at the MP, aligned with the magnetosheath flow, suppressing the development of the KHI. Hence, low angles $\langle \phi_m \rangle$ under slightly negative B_z conditions may be interpreted in terms of the absence of KH waves at the dusk flank MP (see also Figure 1b).

This hypothesis is supported by the fact that a majority of 13 of the 23 groups with $B_z / \sqrt{B_x^2 + B_y^2} < 0$ and $\langle \phi_m \rangle < 90^\circ$ pertain to IMF $B_x < 0$ and $B_y > 0$ or $B_x > 0$ and $B_y < 0$ conditions, so that the quasi-parallel shock is on the dawnside. The magnetosheath field behind that shock is weaker along the flow at the MP, and hence, the amplification of MP surface waves by the KHI should be enhanced [*Nykyri*, 2013]. The dusk flank, where MMS was observing MP waves, was, however, behind the quasi-perpendicular shock in those 13 cases. Another 6 of the 23 groups are associated with strong IMF $|B_x| > 2.8 |B_y|$, i.e., radial IMF that should also be less favorable for KHI development at the equatorial flank MP, although KH waves have been observed under such conditions [*Gratton et al.*, 2012; *Farrugia et al.*, 2014]. In the four remaining cases/groups, B_x and B_y are of equal sign and comparable; hence, the dayside dusk flank MP should have been situated below the quasi-parallel shock.

Finally, we would like to point out that the validity of the results presented in this section is dependent on accurate knowledge (1) of the solar wind conditions and (2) of the angles $\langle \phi_m \rangle$:

1. We have used NASA's OMNI data set to determine the solar wind conditions; this data set is based on measurements by solar wind monitors far upstream of the Earth's bow shock. It is known that the propagation of the measurements to the bow shock nose introduces uncertainty. *Šafránková et al.* [2009], for instance, studied the reliability of the prediction of IMF B_z in the magnetosheath from OMNI data set observations. They found that the sign of $|B_z| < 1$ nT is correctly predicted only 50% of the time and that this prediction may fail even for $|B_z| > 9$ nT.
2. The angles $\langle \phi_m \rangle$ directly depend on the MP model-determined reference normal directions N . If these were systematically tilted toward the $+M/-M$ direction, then there would be a tendency of waves to appear regularly/inversely steepened. The MP model introduced by *Shue et al.* [1998], if correctly used, should be able to yield reference N directions accurate to within a few degrees or better. Otherwise, the model would

not be able to correctly predict the average MP position at the flanks, significantly beyond the terminator, which it demonstrably does. However, a crucial parameter that controls the shape of the model MP is α (see equation (3)). This parameter is a function of IMF B_z and of the solar wind dynamic pressure D_p which may not always be accurately represented by OMNI data set observations, as stated above. In addition, off-center observations of the MP waves should yield angles $\langle\phi_m\rangle$ that are closer to 90° and, hence, contribute to the uncertainty in determining whether $\langle\phi_m\rangle$ is larger or smaller than 90° .

4. Summary and Conclusions

(1) The small-scale tetrahedral configuration of the MMS spacecraft, (2) the high time resolution of the burst FGM, SCM, and merged (combined) data products, and (3) the MMS orbits traversing the dayside dusk flank MP regularly during the first months in science phase (September to November 2015) enable us to routinely ascertain with high accuracy the local boundary inclinations of the MP during the passage of surface waves. On comparing those inclinations with respect to reference MP normals, yielding angles $\langle\phi_m\rangle$, we can categorize the type of steepening of the waves (see Figure 1b), whether it is regular as expected for KH waves or anomalous/inverse, as seen and reported in very few prior instances [Chen *et al.*, 1993; Chen and Kivelson, 1993; Plaschke *et al.*, 2013]. We obtain the following results, which are valid (1) if the solar wind conditions are represented well enough by OMNI data set observations and (2) if the angles $\langle\phi_m\rangle$ are known with sufficient accuracy (to within a few degrees).

The range of inclination values of the leading edges (inbound crossings) is larger than that for the trailing edges (outbound crossings). This can be explained by the KH wave amplification, breaking, and vortex formation for which we expect $\langle\phi_i\rangle > 90^\circ$ (see case 3 in Figure 1b). More than three quarters of the groups (86 out of 111) of MP crossings and, hence, wave intervals exhibit KH wave type steepening, i.e., $\langle\phi_m\rangle > 90^\circ$. The other 25 groups correspond to waves showing inverse steepening. These intervals have to be added to the previously very short list of observations of inversely steepened MP surface waves.

We found the following solar wind conditions to be favorable for the occurrence of inversely steepened waves: (1) dominant IMF $B_z > 0$ as previously seen by Chen *et al.* [1993], Chen and Kivelson [1993], and Plaschke *et al.* [2013]; (2) dominant IMF in the GSM x - y plane. Based on the latter set of conditions, we hypothesize whether the observation of inversely steepened waves is linked to the absence or suppression of KH waves due to the IMF configuration. It should be noted, however, that this hypothesis does not readily explain $\langle\phi_m\rangle < 90^\circ$ unless the seed waves on the MP already feature inverse steepening; it may just explain why KH wave steepening does not develop. Finally, we may also hypothesize whether instabilities arising from the alignment of flow and magnetic field in the magnetosheath might play a role in inverse wave steepening. These instabilities, in contrast, would benefit from relatively low field strengths and high plasma β in the magnetosheath.

Testing of these hypotheses is necessary to ultimately ascertain the reasons for inverse MP wave steepening. Furthermore, that should be possible with MMS observations, on a case-by-case basis, by identifying and analyzing the local plasma and field conditions at/near the MP. Therefore, the data set of inversely steepened MP surface waves resulting from this study should be a valuable starting point.

References

- Angelopoulos, V. (2008), The THEMIS Mission, *Space Sci. Rev.*, *141*, 5–34, doi:10.1007/s11214-008-9336-1.
- Burch, J. L., T. E. Moore, R. B. Torbert, and B. L. Giles (2016), Magnetospheric Multiscale overview and science objectives, *Space Sci. Rev.*, *199*(1), 5–21, doi:10.1007/s11214-015-0164-9.
- Cahill, L. J., and P. G. Amazeen (1963), The boundary of the geomagnetic field, *J. Geophys. Res.*, *68*, 1835–1843, doi:10.1029/JZ068i007p01835.
- Chapman, S., and V. C. A. Ferraro (1930), A new theory of magnetic storms, *Nature*, *126*, 129–130, doi:10.1038/126129a0.
- Chen, S.-H., and M. G. Kivelson (1993), On nonsinusoidal waves at the Earth's magnetopause, *Geophys. Res. Lett.*, *20*, 2699–2702, doi:10.1029/93GL02622.
- Chen, S.-H., M. G. Kivelson, J. T. Gosling, R. J. Walker, and A. J. Lazarus (1993), Anomalous aspects of magnetosheath flow and of the shape and oscillations of the magnetopause during an interval of strongly northward interplanetary magnetic field, *J. Geophys. Res.*, *98*, 5727–5742, doi:10.1029/92JA02263.
- Fairfield, D. H., A. Otto, T. Mukai, S. Kokubun, R. P. Lepping, J. T. Steinberg, A. J. Lazarus, and T. Yamamoto (2000), Geotail observations of the Kelvin-Helmholtz instability at the equatorial magnetotail boundary for parallel northward fields, *J. Geophys. Res.*, *105*(A9), 21,159–21,173, doi:10.1029/1999JA000316.
- Farrugia, C. J., F. T. Gratton, and R. B. Torbert (2001), Viscous-type processes in the solar wind-magnetosphere interaction, *Space Sci. Rev.*, *95*, 443–456.
- Farrugia, C. J., F. T. Gratton, G. Gnani, R. B. Torbert, and L. B. Wilson (2014), A vortical dawn flank boundary layer for near-radial IMF: Wind observations on 24 October 2001, *J. Geophys. Res. Space Physics*, *119*, 4572–4590, doi:10.1002/2013JA019578.

Acknowledgments

The dedication and expertise of the Magnetospheric MultiScale (MMS) development and operations teams are greatly appreciated. Work at JHU/APL, UCLA, UNH, and SwRI was supported by NASA contract NNG04EB99C. We acknowledge the use of merged magnetic field measurements that are based on burst FluxGate Magnetometer (FGM) data from the Digital Flux-Gate (DFG) magnetometers and burst Search Coil Magnetometer (SCM) data. Furthermore, we acknowledge the use of fast survey Fast Plasma Investigation (FPI) data. The FPI data are stored at the MMS Science Data Center <https://lasp.colorado.edu/mms/sdc/> and are publicly available. The merged magnetic field data are available upon request. The Austrian part of the development, operation, and calibration of the DFG was financially supported by rolling grant of the Austrian Academy of Sciences and the Austrian Space Applications Programme with the contract FFG/ASAP-844377.

- Fischer, D., et al. (2016), Optimized merging of search coil and fluxgate data for MMS, *Geosci. Instrum. Methods Data Syst. Discuss.*, 2016, 1–21, doi:10.5194/gi-2016-11.
- Foullon, C., C. J. Farrugia, A. N. Fazakerley, C. J. Owen, F. T. Gratton, and R. B. Torbert (2008), Evolution of Kelvin-Helmholtz activity on the dusk flank magnetopause, *J. Geophys. Res.*, 113, A11203, doi:10.1029/2008JA013175.
- Gratton, F. T., G. Gnani, C. J. Farrugia, L. Bilbao, and R. Torbert (2012), Velocity shear instability and plasma billows at the Earth's magnetic boundary, *J. Phys. Conf. Ser.*, 370(1), 012003, doi:10.1088/1742-6596/370/1/012003.
- Harvey, C. C. (1998), Spatial gradients and the volumetric tensor, *ISSI Sci. R. Ser.*, 1, 307–322.
- Hasegawa, H., M. Fujimoto, T.-D. Phan, H. Rème, A. Balogh, M. W. Dunlop, C. Hashimoto, and R. TanDokoro (2004), Transport of solar wind into Earth's magnetosphere through rolled-up Kelvin-Helmholtz vortices, *Nature*, 430, 755–758, doi:10.1038/nature02799.
- King, J. H., and N. E. Papitashvili (2005), Solar wind spatial scales in and comparisons of hourly Wind and ACE plasma and magnetic field data, *J. Geophys. Res.*, 110, A02104, doi:10.1029/2004JA010649.
- Lavraud, B., J. E. Borovsky, A. J. Ridley, E. W. Pogue, M. F. Thomsen, H. Rème, A. N. Fazakerley, and E. A. Lucek (2007), Strong bulk plasma acceleration in Earth's magnetosheath: A magnetic slingshot effect?, *Geophys. Res. Lett.*, 34, L14102, doi:10.1029/2007GL030024.
- Le Contel, O., et al. (2016), The search-coil magnetometer for MMS, *Space Sci. Rev.*, 199(1), 257–282, doi:10.1007/s11214-014-0096-9.
- Li, W., C. Wang, B. Tang, X. Guo, and D. Lin (2013), Global features of Kelvin-Helmholtz waves at the magnetopause for northward interplanetary magnetic field, *J. Geophys. Res. Space Physics*, 118, 5118–5126, doi:10.1002/jgra.50498.
- Li, W. Y., X. C. Guo, and C. Wang (2012), Spatial distribution of Kelvin-Helmholtz instability at low-latitude boundary layer under different solar wind speed conditions, *J. Geophys. Res.*, 117, A08230, doi:10.1029/2012JA017780.
- Nakamura, T. K., D. Hayashi, M. Fujimoto, and I. Shinohara (2004), Decay of MHD-scale Kelvin-Helmholtz vortices mediated by parasitic electron dynamics, *Phys. Rev. Lett.*, 145001(14), doi:10.1103/PhysRevLett.92.145001.
- Nykyri, K. (2013), Impact of MHD shock physics on magnetosheath asymmetry and Kelvin-Helmholtz instability, *J. Geophys. Res. Space Physics*, 118, 5068–5081, doi:10.1002/jgra.50499.
- Plaschke, F. (2016), ULF waves at the magnetopause, in *Low-Frequency Waves in Space Plasmas*, edited by A. Keiling, D.-H. Lee, and V. Nakariakov, pp. 193–212, John Wiley, Hoboken, N. J., doi:10.1002/9781119055006.ch12.
- Plaschke, F., V. Angelopoulos, and K.-H. Glassmeier (2013), Magnetopause surface waves: THEMIS observations compared to MHD theory, *J. Geophys. Res. Space Physics*, 118, 1483–1499, doi:10.1002/jgra.50147.
- Pollock, C., et al. (2016), Fast plasma investigation for Magnetospheric Multiscale, *Space Sci. Rev.*, 199(1), 331–406, doi:10.1007/s11214-016-0245-4.
- Robert, P., A. Roux, C. C. Harvey, M. W. Dunlop, P. W. Daly, and K.-H. Glassmeier (1998), Tetrahedron geometric factors, *ISSI Sci. Rep. Ser.*, 1, 323–348.
- Russell, C. T., et al. (2016), The Magnetospheric Multiscale magnetometers, *Space Sci. Rev.*, 199(1), 189–256, doi:10.1007/s11214-014-0057-3.
- Shue, J.-H., et al. (1998), Magnetopause location under extreme solar wind conditions, *J. Geophys. Res.*, 103, 17,691–17,700, doi:10.1029/98JA01103.
- Sibeck, D. G., R. P. Lepping, and A. J. Lazarus (1990), Magnetic field line draping in the plasma depletion layer, *J. Geophys. Res.*, 95, 2433–2440, doi:10.1029/JA095iA03p02433.
- Sibeck, D. G., R. E. Lopez, and E. C. Roelof (1991), Solar wind control of the magnetopause shape, location, and motion, *J. Geophys. Res.*, 96, 5489–5495, doi:10.1029/90JA02464.
- Song, P., R. C. Elphic, and C. T. Russell (1988), Multi-spacecraft observations of magnetopause surface waves—ISEE 1 and 2 determinations of amplitude, wavelength and period, *Adv. Space Res.*, 8, 245–248, doi:10.1016/0273-1177(88)90137-8.
- Spreiter, J. R., A. L. Summers, and A. Y. Alksne (1966), Hydromagnetic flow around the magnetosphere, *Planet. Space Sci.*, 14, 223–250, doi:10.1016/0032-0633(66)90124-3.
- Torbert, R. B., et al. (2016), The FIELDS instrument suite on MMS: Scientific objectives, measurements, and data products, *Space Sci. Rev.*, 199(1), 105–135, doi:10.1007/s11214-014-0109-8.
- Šafránková, J., M. Hayosh, O. Gutynska, Němeček, and Přeč (2009), Reliability of prediction of the magnetosheath B_z component from interplanetary magnetic field observations, *J. Geophys. Res.*, 114, A12213, doi:10.1029/2009JA014552.